ce/papers Proceedings in civil engineering

Ernst & Sohn A Wiley Brand

ORIGINAL ARTICLE

eurosteel AMSTERDAM 2023

Ernst & Sohn A Wiley Brand

3D-printing with steel on thin sheets for application in free form façade construction: welding process development and material properties

Philipp Grebner[1] | Jörg Lange[1]

Correspondence

Philipp Grebner, M.Sc.
Technical University Darmstadt
Institute for Steel Construction and Materials Mechanics
Franziska-Braun-Straße 3
64287 Darmstadt
E-Mail: grebner@stahlbau.tu-darmstadt.de

[1] Institute for Steel Construction and Materials Mechanics, Technical University Darmstadt, Darmstadt, Germany

Abstract

Wire and Arc Additive Manufacturing (WAAM) became a significant research field in structural engineering over the past years. It offers the opportunity to apply material fast and precisely, following the load path, inducing effective material consumption. Considering free-formed sheet-metal façades, to date large thicknesses are necessary to maintain the final shape and load-bearing capacity that however causes high material consumption and costs during the construction processes. Hence, WAAM could be an opportunity to reduce the amount of mild steel used for free-form façades. As part of a research project at TU Darmstadt, 1 mm thick free-form sheet-metal façades elements have been manufactured using WAAM. Due to precisely welded lattice structures, placed on the backside of the metal sheet, the reinforcement will be ensured. Wide studies on welding parameters focused on a stable process without damaging the later frontside of the façade panel and on process optimization. In addition, material properties of the welding material have been determined to check its usability in façade construction.

Keywords

WAAM, façade, 3D-printing, process optimization, thin sheets, additive manufacturing, welding, material properties

1 Introduction

The AM process describes the creation of a structure by applying layer by layer of a paste-like or fluid material, which hardens immediately after application [1]. Over almost four decades, additive manufacturing developed and is today used in several fields, such as aerospace, civil engineering, or medicine. As the three industry areas already indicate, the applied material variation is diverse. In research and industry materials like steel, polymers, sand and concrete are commonly used [2–4]. Among the advantages of additive manufacturing, less material consumption and manufacturing time savings are to be mentioned in comparison to subtractive manufacturing methods. In addition, those two factors can result in significant cost savings [5].

1.1 Wire Arc Additive Manufacturing

Wire Arc Additive Manufacturing (WAAM) is one method for 3D-printing with steel. The 3D-printing system consists of a gas shielded metal arc welding device (GMAW) and a robotic or gantry system [6]. WAAM is the commonly used additive manufacturing method in steel construction research due to its high deposition rates and at the same time sufficient accuracy for constructional steel applications. The alloys of the welding wires vary from unalloyed mild steel to high alloyed wires. The shielding gases used, corresponding to the wire, are inert gases like Argon or Helium or gas mixtures with oxidative active gases [7].

1.2 Free form sheet metal façade constructions

To date, there are already a few examples for free-form sheet metal façades: the Cloud Gate sculpture in Chicago (figure 1) [8], the Zahner ZEPPS façade system [9], or the composite façade system Alucobond [10]. The problems of those systems are that they have either high material consumption, expensive materials like aluminium, composites difficult to recycle or complex substructures (figure 2), which make them more expensive. Using WAAM to reinforce thin mild steel sheets with a mild steel welding wire, could be a more economic and ecologic solution to fabricate free form sheet metal façades, causing low material consumption using only mild steel [11].

https://doi.org/10.1002/cepa.2299 wileyonlinelibrary.com/journal/cepa

Figure 1 Cloud Gate, Chicago

Figure 2 Sub construction Cloud Gate, Chicago [12]

1.3 Welding distortions

Probably the most important problem during welding on thin sheets is to handle thermal induced distortions due to material shrinking. There are several types of welding distortions as shown in figure 3 [13]. All types shown are interacting when a weld seam is applied, but buckling is the most unpredictable form of welding distortion. To reduce distortions, pre-bending might be a solution. Furthermore, using a CO_2-snow cooling directly behind the welding gun can reduce welding distortions significantly [13]. In addition, Smith et al. tried to quantify welding induced residual stresses numerically and experimentally [14].

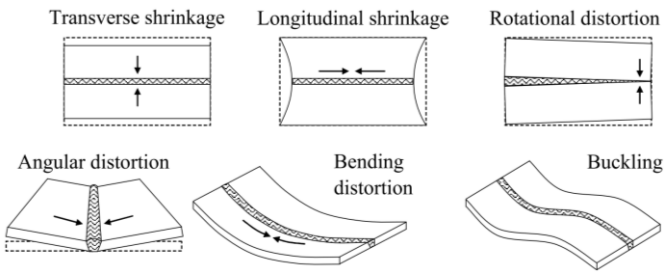

Figure 3 Different types of welding distortions [14]

2 Welding process development

Using WAAM to reinforce thin sheets means finding a way to accept or even integrate welding induced distortions as a design factor. Quantifying residual stresses or different types of bending in a unique reinforcement on the backside of a free form façade panel yet seems not realistic. In addition, using CO_2-snow cooling for WAAM requires a second robotic system and is ecologically unacceptable. However, to achieve the intended shape of a free form façade panel, a reinforcing welding process should induce as little distortion as possible. Therefore, the heat input of different welding parameters can be quantified by measuring one of the occurring welding distortions after welding a straight line on a piece of thin sheet metal. Besides the distortion, two other factors should be considered. First, the welding process must not burn through the thin sheet, which would make the façade panel unusable. Second, the process must be applicable to be used for a multilayer reinforcement.

The WAAM system used at TU Darmstadt is a Comau NM 16-3.1 six axis industry robot working with a Fronius CMT Advanced 4000 R welding device shown in figure 4. To minimize the heat input, the smallest possible wire diameter of 0.8 mm is used with a WDI Weko 2 G3Si1 wire electrode, suitable for normal strength mild steels as base material. As shielding gas, a Messer Ferroline C18 (82 % Ar, 18 % CO_2) is used.

Figure 4 WAAM laboratory at TU Darmstadt [16]

2.1 CMT Cycle-Step welding process

The CMT Cycle-Step welding process is a modified short electric arc welding process from Fronius GmbH [15]. The process is based on a continuous alternating movement of the welding wire during the process. The wire moves towards the base material and drops the melted material into the weld pool by performing a rapid backwards movement. Thereby, no additional pinch force is needed to release the molten droplet. Additionally, the amount of molten material can be controlled by the number of cycles within a Cycle-Interval. Also, an interval break between every Cycle-Interval can be used to adjust the amount of material, heat input, and height of a welded seam [15].

2.2 Characteristic curve selection

Every welding process relates to a characteristic curve. The characteristic curve (CC) contains parameters to weld with a certain wire diameter and material in a defined Wire

Feed Speed (WFS) range. To find a parameter set to weld on thin sheets, a suitable CC has to be found. To date, Fronius does not offer a CMT Cycle-Step CC for 0.8 mm G3Si1 wire. Therefore, five possible CC options for different alloyed steels and wire diameters have been selected. They are listed in table 1 with their number related to the Fronius database.

Table 1 Selected characteristic curves

CC Nr.	Nominal Material	Nominal Wire diameter in mm	min. WFS in m/min	Distortion d measured in mm
1872	G3Si1	1.0	0.6	5
1006	A DUR 600	0.8	0.5	3
1863	NiFeCr-2	0.8	0.5	2.5
1752	Ti-5	0.8	0.5	1.1

Table 2 Welding parameters

Travel speed in mm/s	Cycles	Interval break in ms	CTWD in mm	Shielding gas
500	2	4	10	C18

Afterwards, an 11 x 20 cm mild steel sheet with a thickness of 1.0 mm has been clamped on its longitudinal sides to prevent distortions during the welding process (figure 5). In the next step a 16 cm weld seam has been applied for each of the characteristic curves. Thereby, the minimum WFS of each CC has been selected (table 1). Other welding parameters are listed in in table 2. After the welding, one side of the clamping has been released, and the distortion d due to angular distortion has been measured centric on the released edge of the sheet (figure 5, table 1). The Characteristic curve 1752 with the lowest distortion has been selected for further testing to minimize distortions. Furthermore, CC 1872 has also been selected with the idea to weld with a small number of cycles using a CC with a higher heat input supposed for 1.0 mm wire diameter. Figure 6 shows the welding process for the distortion measurement test.

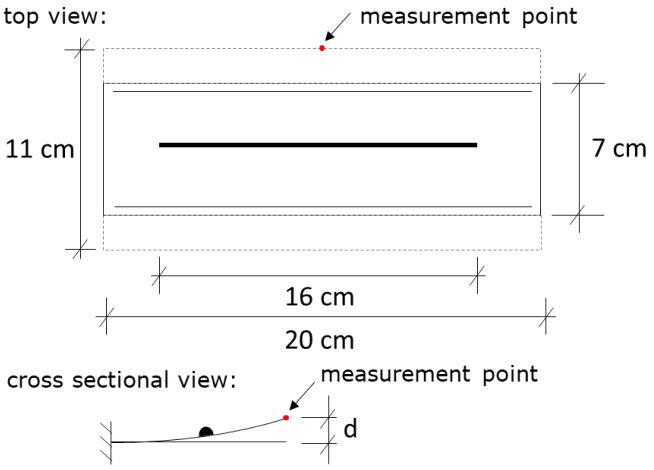

Figure 5 Setup of the distortion measurement

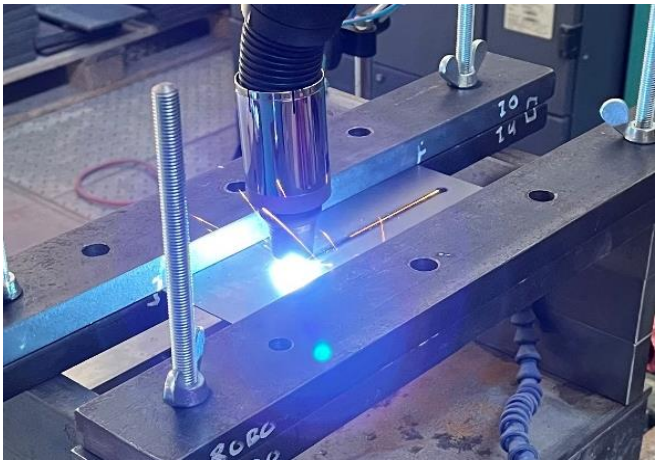

Figure 6 Robot welding one seam for the distortion measurement

In a next step, the welding parameters of the two characteristic curves have been adjusted with the objective to receive a parameter set which is suitable to build layer by layer structures and thereby not burning through the sheet metal. Therefore, the following parameters Wire Feed Speed (WS), Travel Speed (TS), interval break and cycles have been adjusted incrementally (Table 3).

Table 3 Adjusted welding parameters

CC Nr.	WFS	TS in mm/min	Interval break in ms	cycles
1872	3.6	450	4	2
1752	0.5	350	0	15

Both parameters are shown on the front- and backside of the thin sheet in Figure 7 and 8.

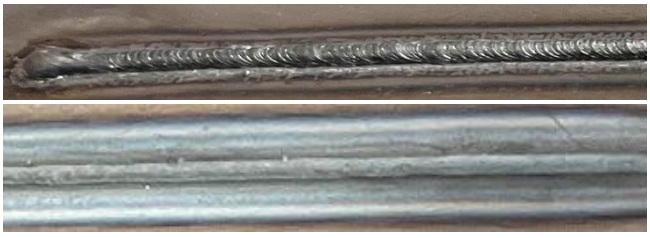

Figure 7 Parameter of CC 1872, frontside (a), backside (b)

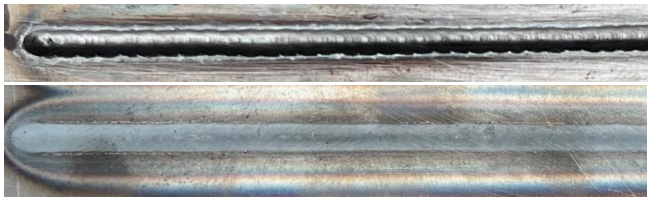

Figure 8 Parameter of CC 1752, frontside (a), backside (b)

Also, both parameters can be welded in several layers. To decide between both parameters, the flexibility of both have been tested by changing the robot travel speed in a range of ± 100 mm/min. The result has shown that parameter set 1872 is more suitable for application in WAAM. Parameter set 1752 has shown a burn through for lower travel speeds and has led to an unstable process.

In further optimizations the welding start parameters have been adjusted to ensure no welding mistakes in the starting point area. Therefore, the Special-Two-Step mode [15] from Fronius has been used to successively adjust the welding start current (I_s) and time (t_s) as well as the transition time to normal welding current, called slope (sl_1). Figure 9a and b show the welded parameter set before and after the optimization. Table 4 shows the adjusted values.

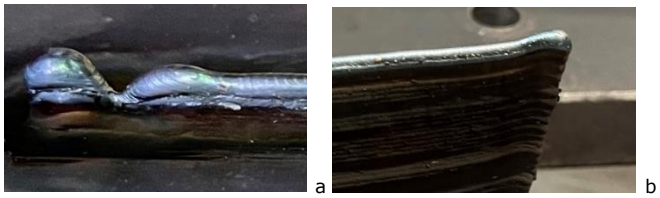

Figure 9 Parameter optimization with the Special-Two-Step

Table 4 Adjusted Special-Two-Step parameters

CC Nr.	I_s in %	t_s in s	sl_1 in s
1872	70	0,3	0,7

Due to the low deposition rate of the selected welding parameter set, two process optimization tasks are remaining. First, there must be a slicing strategy found to connect crossing welding seams. First tests, using recent research results [17–19] have not led to satisfactory results. Furthermore, a way to fill up gaps due to random welding mistakes must be found. Therefore, a standard short arc welding process could be a solution to fill small gaps while the alternating wire movement in the CMT-process causes problems with the electric arc not hitting the gap.

3 Material properties

To validate the usability of the developed welding parameter set, material properties have been determined. Therefore, six strain-controlled tensile strength tests, according to DIN EN ISO 6892-1, have been performed. The tensile specimens have been taken out of two 100-layer walls as shown in figure 10.

Figure 10 100-layer wall (a) and tensile specimen (b)

Due to a gross material thickness a_0 between 1.8 – 2.5 mm, measured using a micrometer with spikes to reach the smallest thickness in the gap between the layers, the tensile specimen p.1 to p.6 have to be pulled "as built" without being milled on a defined thickness before testing. A parallel length l_0 of 5 cm has been ensured by slightly milling the sides to a constant width b of 2.0 cm. Figure 11 shows the stress strain curves of all six specimens. The stresses in the specimens were calculated using the measured load by the test stand, the parallel length l_o and the smallest measured thickness a_0 of each specimen.

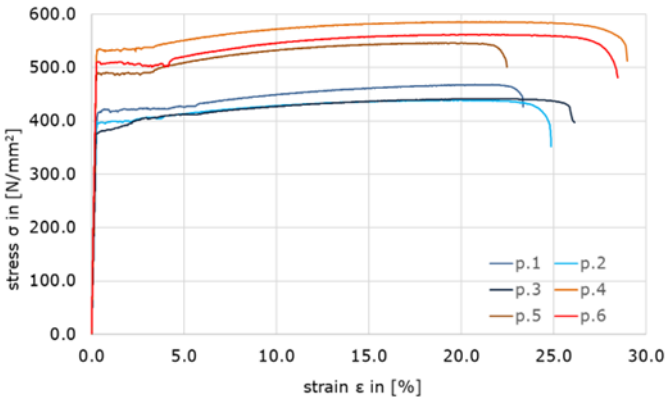

Figure 11 Stress strain diagram of p.1 – p.6

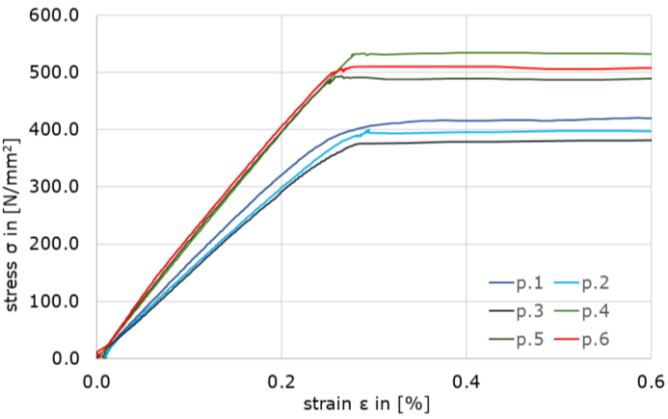

Figure 12 Linear elastic section of the stress strain diagram of p.1 – p.6

Average values for yield strength f_y, ultimate strength f_u, fracture strain A and Young's modulus E are shown in table 5. The differences between the values of p.1-p.3 and p.4-p.6 could be traced back on the fact that there are differences in the thickness. P.1-p.3 show an average thickness of 2.4 mm while p.4-p.6 reaches only 1.9 mm. Though, different interpass cooling to 100°C has be applied for p.1-

p.3 and p.4-p.6. Specimens p.1-p.3 have been cooled down for 60 s by room temperature, while p.4-p.6 have been cooled down for 15 s by a high pressure-air-water mixture. Figure 12 shows the linear elastic section of the tensile specimen to show the differences of the gradients between p.1-p.3 and p.4-p.6.

Table 5 Material properties

Nr.	E in N/mm²	f_y in N/mm²	f_u in N/mm²	A in %
p.1 – p.3	155374	404.3	499.2	24
p.4 – p.6	193491	511.9	564.3	26

The linear elastic sections seem to overlap in figure 11 but a difference is noticeable considering figure 12 and the differences in the Young's modulus in table 5. Reaching the yield strength, the specimens start to plasticize while there is only a low stress increase. After passing the ultimate strength there is almost no necking before the specimens fail.

The results show similar material behavior in both, elastic and plastic sections. The material has less plastic load-bearing capacities compared to normal strength mild steels, which reach a strength ratio f_u/f_y up to 1.5 compared to the welded material reached only a strength ratio of 1.24 in p.1-p.3 and 1.10 in p.4-p.6.

The influence of different interpass cooling methods show an influence on the material strengths and stiffness. Considering the Young's Modulus, the pressure-air-water cooled specimens p.4-p.6 show a higher stiffness than the not active cooled specimens p.1-p.3. Furthermore, the active cooled specimens show an increased yield and ultimate strength. Also, the active cooled specimens show a decreased material thickness.

To compare the welded material with thin sheets of mild steel, in addition three tensile specimens of a S355 1.0 mm sheet metal have been tested. The average material properties of all welding material and sheet metal specimens are shown in table 6. The yield strength of the welded material reaches significantly higher values than the sheet metal. Looking at the Young's modulus common mild steels reach a higher stiffness than the welded material. Comparing the fracture strains, both materials show similar values. As expected, the ultimate strength of the sheet metal is higher than the ultimate strength of the welded material due to the low plastic load-bearing capacity of the welded material.

Table 6 material properties of the welded material and shin sheet metal

Nr.	E in N/mm²	f_y in N/mm²	f_u in N/mm²	A in %
p.1 – p.6	174433	458.1	506.8	25
sheet metal	208434	366.3	635.3	25

4 Conclusion

This paper explains the process of a welding parameter development for reinforced thin sheets with WAAM for application in free form façade construction. Two characteristic curves (CC) with a minimum distortion have been chosen and further parameter adjustments have led to the decision for the parameter set based on characteristic curve 1872 from Fronius. Further optimizations at the welding start have been made to avoid welding mistakes. Material properties of the welded material have been determined. The average yield strength and strain values are comparable with those of S355 sheet metal. The welding material shows less plastic load-bearing capacity than the sheet metal. High pressure-air-water interpass cooling seems to have a hardening and stiffening effect increasing the yield and ultimate strength and the Young's modulus of the welding material. Considering the design of a façade panel of approximately 1.0x2.0 m for typical wind loads according to Eurocode 1 - 4, which reach approximately 1 kN/m² in urban areas of Germany, it can be assumed that a WAAM reinforced façade panel can withstand the expected loads by defining a sufficient layer height. A suitable rib arrangement could be used to assume a beam load-bearing behavior for the ribs. Further studies should therefore focus on component testing and numerical analysis. In addition, studies on finding slicing strategies for crossing welding seams should be carried out. Finally, a way to mill the welded material could provide better tensile strength specimens to avoid "as built" testing.

Acknowledgements We want to thank the companies Fronius Deutschland GmbH, Messer Group GmbH and WDI - Westfälische Drahtindustrie GmbH for their continuous and active support during our research. This research has been funded by the Bundesministerium für Wirtschaft und Klimaschutz (project number: 03LB3048D).

References

[1] Gebhardt, A. (2016) Additive Fertigungsverfahren – Additive Manufacturing und 3D-Drucken für Prototyping - Tooling - Produktion. 5. Aufl. München: Hanser.

[2] Krause, M. (2021) Baubetriebliche Optimierung des vollwandigen Beton-3D-Drucks. Wiesbaden: Springer Fachmedien Wiesbaden.

[3] MX3D (2019) Connector for Takenaka [online]. https://mx3d.com/industries/construction/connector-for-takenaka/ [Zugriff am: 10. Okt. 2021].

[4] Weger, D. et al. (2021) Building rethought – 3D concrete printing in building practice in: Construction Robotics 5, 3-4, S. 203–210. https://doi.org/10.1007/s41693-022-00064-5

[5] Lachmayer, R.; Lippert, R. B.; Kaierle, S. (2018) Additive Serienfertigung. Berlin, Heidelberg: Springer Berlin Heidelberg.

[6] Williams, S. W. et al. (2016) Wire + Arc Additive Manufacturing in: Materials Science and Technology 32, H. 7, S. 641–647. https://doi.org/10.1179/1743284715Y.0000000073

[7] Schuler, V.; Twrdek, J. (2019) Praxiswissen Schweiß-

technik. Wiesbaden: Springer Fachmedien Wiesbaden.

[8] City of Chicago (2006) Cloud Gate in Millennium Park [online]. https://www.chicago.gov/city/en/depts/dca/supp _info/chicago_s_publicartcloudgateinmillenniumpark.html [Zugriff am: 21. Mrz. 2023].

[9] Zahner Company, A. ZEPPS (Zahner Engineered Profile Panel System) [online]. https://zahner-wordpress-media.s3.amazonaws.com/wp-content/uploads/2021/02/22141208/ZDS-ZEPPS-210218.pdf [Zugriff am: 21. Mrz. 2023].

[10] 3A Composites GmbH Alucobond [online]. https://alucobond.com/cms/deliver/ALUCOBOND_Facade_fascination_DE.pdf [Zugriff am: 21. Mrz. 2023].

[11] Bergmann, J. P. et al. (2018) Grundlegende wissenschaftliche Konzepterstellung zu bestehenden Herausforderungen und Perspektiven für die Additive Fertigung mit Lichtbogen – Studie im Auftrag der Forschungsvereinigung Schweißen und verwandte Verfahren e.V. des DVS. Düsseldorf: DVS Media GmbH.

[12] Public Domain Pictures Cloud Gate in Chicago [online]. https://www.publicdomainpictures.net/de/view-image.php?image=198609&picture=chicago-cloud-gate [Zugriff am: 23. Mrz. 2023].

[13] van der Aa, E. M. (2007) Local Cooling during Welding – Prediction and Control of Residual Stresses and Buckling Distortion. Delft: Delft University of Technology.

[14] Smith, M. C.; Akrivos, V.; Vasileiou, A. (2018) How reliable are prediction and measurement of weld residual stresses - lessons from the NeT network. Manchester: The University of Manchester.

[15] Fronius GmbH operating instructions - TPSi [online]. file:///C:/Users/Philipp%20Grebner/Downloads/42,0426,0114,DE.pdf [Zugriff am: 21. Mrz. 2023].

[16] Waldschmitt, B. et al. (2022) 3d printing of column structures for architectural applications in: Architecture, Structures and Construction 2, H. 4, S. 565–574. https://doi.org/10.1007/s44150-022-00050-z

[17] Ding, D. et al. (2015) A multi-bead overlapping model for robotic wire and arc additive manufacturing (WAAM) in: Robotics and Computer-Integrated Manufacturing 31, S. 101–110. https://doi.org/10.1016/j.rcim.2014.08.008

[18] Hu, Z. et al. (2020) Multi-bead overlapping model with varying cross-section profile for robotic GMAW-based additive manufacturing in: Journal of Intelligent Manufacturing 31, H. 5, S. 1133–1147. https://doi.org/10.1007/s10845-019-01501-z

[19] Xiong, J. et al. (2013) Modeling of bead section profile and overlapping beads with experimental validation for robotic GMAW-based rapid manufacturing in: Robotics and Computer-Integrated Manufacturing 29, H. 2, S. 417–423. https://doi.org/10.1016/j.rcim.2012.09.011